


 Cite this: *RSC Adv.*, 2024, 14, 7258

 Received 13th December 2023  
 Accepted 16th February 2024

DOI: 10.1039/d3ra08519h

[rsc.li/rsc-advances](https://rsc.li/rsc-advances)

# Mechanochromic aromatic hydrocarbons that bear one simple substituent†

 Tomohiro Seki \* and Kota Hattori

Structurally simple aromatic hydrocarbons that possess only one isocyano group show luminescent mechanochromism. The structural isomers of these aromatic hydrocarbons exhibit blue- and red-shifted emission bands upon mechanical stress. Their low molecular weight enables their sublimation under mild conditions.

Luminescent mechanochromism is a phenomenon that involves an emission-color change in solids or liquid crystals induced by mechanical stimulation such as grinding and pressing.<sup>1–4</sup> Various organic and organometallic compounds have been reported to show luminescent mechanochromism.<sup>5–13</sup> So far, a variety of strategies have been developed to generate mechanochromic compounds, including the use of multiple intermolecular interactions,<sup>7,14,15</sup> connection of donor and acceptor units,<sup>16,17</sup> controlling dipole moments,<sup>18</sup> and switching between monomeric and assembled states.<sup>19</sup> However, these strategies require mechanochromic compounds with rather complicated molecular structures; thus, low-molecular-weight mechanochromic compounds are still scarce.

Polycyclic aromatic hydrocarbons (PAHs) such as anthracene,<sup>20–22</sup> pyrene,<sup>7,23–26</sup> and perylene<sup>27–29</sup> are among the structurally simplest mechanochromic compounds. These PAHs contain a variety of functional substituents, such as amide, cyano, boronic ester, and alkyl groups and/or linkages to other aromatic or heteroaromatic groups. However, except for an unusual example,<sup>30</sup> reports that describe unsubstituted PAHs show luminescent mechanochromism remain elusive. This indicates that the introduction of several substituents or connection to the same or other  $\pi$ -conjugated groups is required to endow simple PAHs with mechanochromic properties. Especially mechanochromic PAHs that bear only one simple substituent remain a rarity.<sup>31</sup>

Here, we report structurally simple monosubstituted pyrene isomers **1** and **4**, which exhibit luminescent mechanochromism. Compared with other reported mechanochromic compounds, the chemical structures of **1** and **4** are relatively simple, *i.e.*, they contain only one isocyano group as a substituent and their molecular weight is low (MW = 227). Solid

samples of **1** and **4** exhibit luminescent mechanochromism with blue- and red-shifted emission bands, respectively. X-ray diffraction (XRD) analyses indicated that the ground phase of **1** is a crystalline phase, while that of **4** is an amorphous phase. The crystal structures revealed the presence of moderate dipole-dipole interactions in the ground phases compared to those in their pristine phases, which is the key for the mechanochromism of **1** and **4**.

Pyrene **4** was prepared from 4-nitropyrene according to a previously reported procedure for monoisocyano PAHs (for details, see the ESI†).<sup>32</sup> Pyrene **1**, which has already been reported, was prepared in a similar manner.<sup>33</sup> Although **1** was reported not to show luminescent mechanochromism,<sup>33</sup> we found that both **1** and **4** exhibit luminescent mechanochromic properties.

Under excitation at 365 nm, solid samples of pristine **1** and **4** emit green and blue photoluminescence, respectively (Fig. 1). Crystalline **1** shows an intense green emission with an absolute emission quantum yield ( $\Phi_{\text{em}}$ ) of 48% (Table S1†) and an unstructured emission spectrum with a peak at 495 nm (Fig. 2a). Compared with the structured emission of monomeric **1** in  $\text{CH}_2\text{Cl}_2$  ( $c = 5 \mu\text{M}$ , Fig. S1b and S2†), the emission maximum wavelength ( $\lambda_{\text{em,max}}$ ) of **1** in the solid state is red-shifted. The average emission lifetime ( $\tau_{\text{av}}$ ) of pristine solid **1** is 61 ns, which is longer than that of monomeric **1** in  $\text{CH}_2\text{Cl}_2$  (13 ns; Fig. S3a and Table S1†). This indicates that the emission of **1** should be characterized as excimer fluorescence.<sup>23,24,34</sup> Meanwhile, pyrene **4** shows blue emission upon photoexcitation (Fig. 1) with an  $\Phi_{\text{em}}$  of 51% (Table S1†) and a broad emission spectrum with a  $\lambda_{\text{em,max}}$  of 452 nm (Fig. 2b), which is shorter than that of **1**. An emission-decay analysis indicated that the  $\tau_{\text{av}}$  of **4** is 38 ns (Fig. S3b and Table S1†), revealing its excimer character.<sup>23,24,34</sup> The longer  $\lambda_{\text{em,max}}$  and  $\tau_{\text{av}}$  of the excimer emission of **1** compared with those of **4** could stem from the stronger interactions of **1** in the excited state.<sup>35</sup>

To investigate the difference between the  $\lambda_{\text{em,max}}$  of pristine **1** and **4**, single-crystal XRD analyses were performed. A single crystal of **1** was obtained from the vapor-diffusion method using  $\text{CHCl}_3$  and *n*-pentane. Compound **1** crystallizes in the triclinic *P*1

Department of Chemistry, Faculty of Science, Shizuoka University, Shizuoka 422-8017, Japan. E-mail: [seki.tomohiro@shizuoka.ac.jp](mailto:seki.tomohiro@shizuoka.ac.jp)

† Electronic supplementary information (ESI) available: X-ray crystallographic data, optical-microscopy images, thermal data, emission spectra, and other additional information. CCDC 2312583. For ESI and crystallographic data in CIF or other electronic format see DOI: <https://doi.org/10.1039/d3ra08519h>



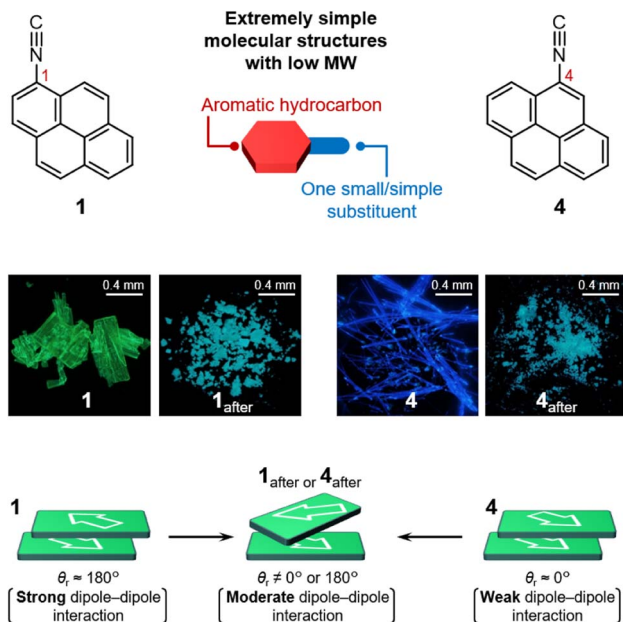


Fig. 1 Chemical structures of **1** and **4**. Photographs of **1**, **1<sub>after</sub>**, **4**, and **4<sub>after</sub>** taken under UV light ( $\lambda_{\text{ex}} = 365$  nm). Schematic representation of stacked dimers of **1**, **1<sub>after</sub>**, **4**, and **4<sub>after</sub>**. Rotation angles of the dipoles of the molecules within the dimer are depicted as  $\theta_r$ .

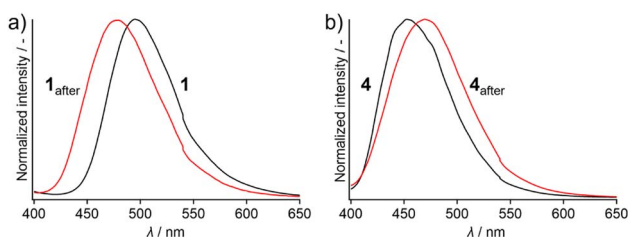


Fig. 2 Emission spectra of solid samples of (a) **1** and **1<sub>after</sub>** and (b) **4** and **4<sub>after</sub>** upon excitation at 365 nm.

space group (Fig. 3a and S5 as well as Table S2<sup>†</sup>).<sup>33</sup> As typically observed for the crystal structures of flat  $\pi$ -systems,<sup>36,37</sup> **1** adopts a co-facial stacking arrangement in a head-to-tail manner with a rotational angle of the isocyanide groups ( $\theta_r$ ) of  $\sim 180^\circ$  (Fig. 3a). These molecules form a one-dimensional (1D) column with an offset along the long axis of the pyrene core ( $20.97^\circ$ ; Fig. 3a and S5<sup>†</sup>) and a short distance of  $\sim 3.44$  Å between the pyrene cores. Single crystals of **4** were also obtained using the vapor-diffusion method with  $\text{CHCl}_3$  and *n*-pentane. Compound **4** crystallizes in the monoclinic  $P2_1/c$  space group (Fig. 3b and S6 as well as Table S2<sup>†</sup>) and also adopts a stacking arrangement to form a column with a longitudinal offset along the molecular long axis ( $25.08^\circ$ ; Fig. 3b and S6<sup>†</sup>) similar to that of **1**. However, head-to-head arrangements ( $\theta_r \approx 0^\circ$ ) within the column were confirmed for **4** despite the presence of the electron-withdrawing isocyanide group (the dipole moment of **4** was estimated to be 4.41 D *via* DFT calculations; Fig. S7<sup>†</sup>). However, the stacking distance between molecules of **4** is relatively short ( $\sim 3.43$  Å), which is almost identical to that of **1** with  $\theta_r \approx 180^\circ$ . Thus, the dipole

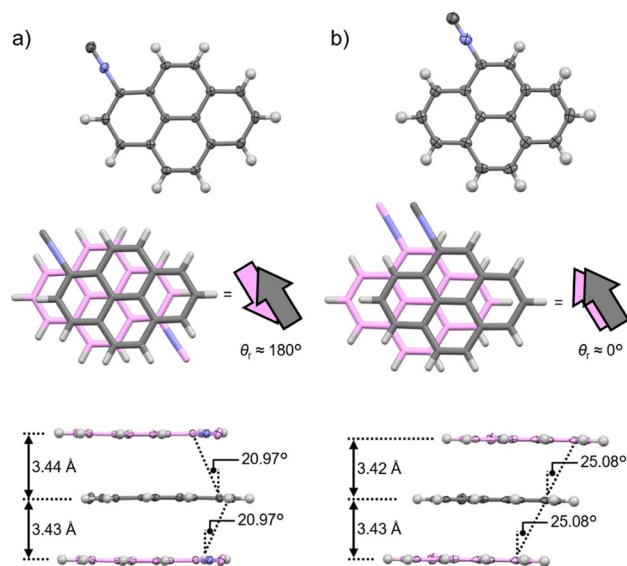


Fig. 3 Molecular structures of (a) **1** and (b) **4** in the single crystal.

moment of **4** should be cancelled out along the *bc* plane, *i.e.*, orthogonal to the stacking direction (Fig. S8<sup>†</sup>).

The different stacking arrangements of **1** (head-to-tail) and **4** (head-to-head) are most likely responsible for their different  $\lambda_{\text{em,max}}$ . Considering that the  $\pi$ -stacking distance and offset angles within the co-facial 1D columns of **1** (3.44 Å and  $20.97^\circ$ , respectively) and **4** (3.43 Å and  $25.08^\circ$ , respectively) are close, a similar degree of excimer formation would be expected. However, the  $\lambda_{\text{em,max}}$  of **1** (495 nm) is longer than that of **4** (452 nm), which can be attributed to the stronger dipole-dipole interactions of the former as revealed by its head-to-tail arrangement ( $\theta_r \approx 180^\circ$ ). Indeed, structurally simple anthracene molecules have been reported to show longer wavelength emission when excimer formation is assisted by dipole-dipole interactions within the stacked dimers.<sup>37</sup> The stronger excimer-like character for the emission of **1** compared to that of **4** is supported by the longer emission lifetime of the former compared to that of the latter (Fig. S3 and Table S1<sup>†</sup>).

Upon grinding, the emission band of **1** was blue-shifted whereas that of **4** was red-shifted. Upon applying mechanical stimulation using a spatula, the emission color of **1** changed from green to light blue (Fig. 1). The resulting powder, **1<sub>after</sub>**, showed a broad emission band with a  $\lambda_{\text{em,max}}$  of 478 nm (Fig. 2a). Such a blue-shifted emission induced by grinding is less common for luminescent mechanochromic compounds<sup>38,39</sup> than a corresponding red-shifted emission. The ground powder of **1<sub>after</sub>** showed an  $\Phi_{\text{em}}$  of 37% and an  $\tau_{\text{av}}$  of 45 ns, indicating excimer-emission character (Fig. S9a and Table S3<sup>†</sup>).<sup>23,24,34</sup> In contrast, when pristine **4** was mechanically ground, a red-shifted emission band was observed (Fig. 2b). The ground powder of **4** (**4<sub>after</sub>**) showed light-blue emission (Fig. 1) with an  $\Phi_{\text{em}}$  of 33% and an  $\tau_{\text{av}}$  of 31 ns (Fig. S9b and Table S3<sup>†</sup>). This long emission lifetime was attributed to excimer emission.<sup>23,24,34</sup> The emission spectrum of **4<sub>after</sub>** is broad and has a maximum at 470 nm, similar to that of **1<sub>after</sub>** ( $\lambda_{\text{em,max}} = 478$  nm; Fig. 2).



Importantly, we confirmed that unsubstituted pyrene molecules exhibit no mechanochromic properties (Fig. S10†), indicating that the introduction of the single isocyno group endows **1** and **4** with mechanochromic properties.

Powder XRD (PXRD) analyses indicated that **1**<sub>after</sub> forms a crystalline phase, while **4**<sub>after</sub> forms an amorphous phase. The PXRD patterns of **1**<sub>after</sub> and **4**<sub>after</sub> were compared with those simulated for the corresponding pristine phases derived from the single-crystal coordinates. The simulated pattern of **1** shows three intense diffraction peaks at 9.40°, 10.93°, and 12.10° (black line in Fig. 4a). After applying stress for a short time, new crystalline peaks appeared at 9.47°, 11.31°, and 12.35°, while the original diffraction peaks of **1** remained as shoulders (yellow line in Fig. 4a). This result implies the coexistence of two different crystalline structures of **1** in an intermediate state.<sup>40</sup> After thorough grinding, the residual shoulders derived from the pristine molecular arrangement disappeared (red line in Fig. 4a), suggesting that the mechanochromism of **1** is based on a crystal-to-crystal phase transition, which is an uncommon phase transition for mechanochromic compounds.<sup>9,13,25,41,42</sup> Conversely, upon mechanical stimulation of **4**, the intensity of the diffraction peaks (*i.e.*,  $2\theta = 10^\circ\text{--}12^\circ$ ) of pristine **4** (black line in Fig. 4b) decreased significantly in ground **4**<sub>after</sub> and no new diffraction peaks emerged (red line in Fig. 4b). This result

indicates that a crystal-to-amorphous phase transition is the origin of the mechanochromism of **4**, which is typically observed for this class of materials.<sup>8–12,15–17,21,28,39,43,44</sup>

In ground-phase **1**<sub>after</sub> and **4**<sub>after</sub>, “moderate” dipole–dipole interactions might be formed compared to pristine **1** and **4**. As mentioned above, the dipole–dipole interactions along the stacking direction in the crystalline phases of **1** and **4** are strong and weak, respectively, as reflected in their corresponding  $\theta_r$  values ( $\sim 180^\circ$  for **1** and  $\sim 0^\circ$  for **4**). These extreme  $\theta_r$  values of the unground phases should become moderate ( $\theta_r \neq 0^\circ$  or  $180^\circ$ ) upon phase transition into the ground phases irrespective of the crystalline (**1**<sub>after</sub>) or amorphous phases (**4**<sub>after</sub>, Fig. 5). This result indicates that the dipole–dipole interactions are most likely weakened after the phase transition from **1** and strengthened from **4** in terms of  $\theta_r$ , upon grinding (Fig. 5). This is consistent with the blue-shifted emission of **1** and the red-shifted emission of **4**. Generally, in addition to  $\theta_r$ , dipole–dipole interactions are also affected by the torsional angles and distance between the  $\pi$  planes relative to the stacking direction (Fig. S11†).<sup>45</sup> However, the lack of a detailed crystal-structure analysis for unknown crystalline **1**<sub>after</sub> and amorphous **4**<sub>after</sub> at this stage hindered unveiling the effect of the torsional angles and distances on the emission wavelength.

Upon thermal treatment, pristine **1** and **4** exhibited a similar behavior to that induced by mechanical stimulation. Thus, heating a pristine solid sample of **1** to 100 °C resulted in an emission-color change from green to light blue (Fig. S12a†). The resulting light-blue emission of **1** remained intact upon cooling to room temperature (Fig. S12a†). The light-blue-emitting crystals of **1** can be regarded as **1**<sub>after</sub> because their emission spectrum and PXRD patterns are similar to those of **1**<sub>after</sub> obtained from mechanical stimulation (Fig. S12b and S12c†). Differential-scanning-calorimetry (DSC) studies of **1** confirmed a thermal phase-transition temperature of 100 °C (Fig. S13 and S14†).<sup>46</sup> Similar to **1**, a solid sample of **4** showed thermoresponsive behavior similar to that observed upon mechanical stimulation, *i.e.*, thermo-induced amorphization of **4** led to a red-shifted emission band (Fig. S15†). These results indicate that mechanical stimulation and thermal treatment induce the same phase transitions in **1** and **4**, leading to clear luminescent chromic behavior.

Compounds **1** and **4** are the luminescent mechanochromic compounds with one of the lowest molecular weights (MW = 227) reported to date.<sup>47</sup> Accordingly, we expected that it should be possible to sublime **1** and **4** under mild conditions,

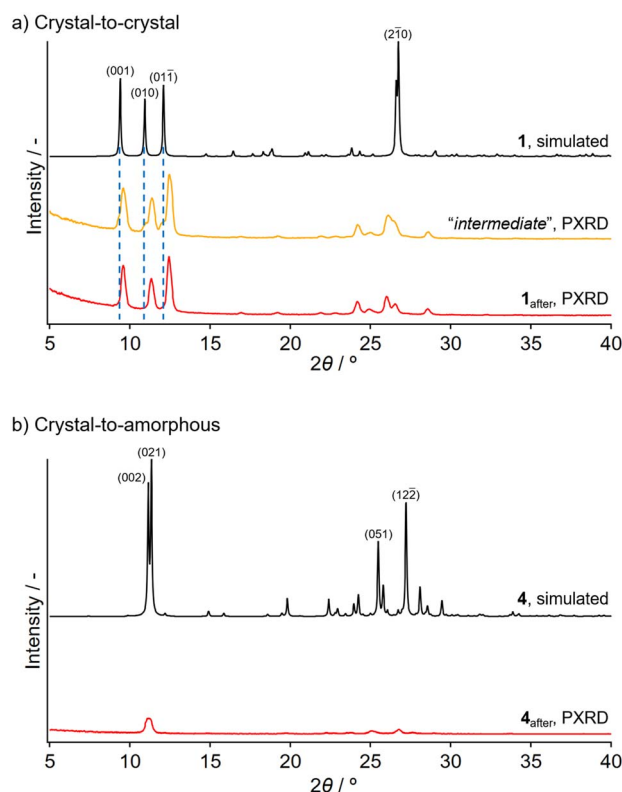


Fig. 4 Simulated PXRD patterns of pristine forms derived from the single-crystal structures (black lines) and experimental PXRD patterns of the ground powders (red lines) of (a) **1** and (b) **4**. The yellow line in (a) is the PXRD pattern of the “intermediate” sample of **1**, which was obtained from grinding for a short time. Miller indices are shown for four intense diffraction peaks of the simulated powder patterns of **1** and **4**.

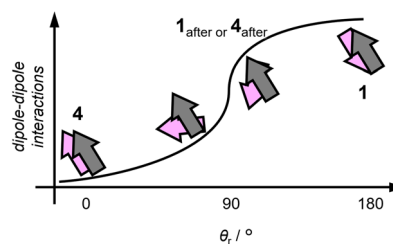


Fig. 5 Schematic representation of the relationship of  $\theta_r$  within the co-facial arrangements of the dipoles (depicted by arrows) in the stacked dimer and the strength of the dipole–dipole interactions.



potentially enabling the low-cost preparation of thin films. To confirm this hypothesis, we conducted preliminary sublimation experiments. After placing a solid sample of **1** in a round bottom flask and reducing the pressure to 2.5 mbar while slowly increasing the temperature, sublimation started at 40 °C (Fig. S16a†). <sup>1</sup>H NMR and polarized-optical-microscopy analyses confirmed that the sublimated solid is **1**, *i.e.*, **1** did not undergo decomposition and maintained crystallinity (Fig. S16b and S17†).<sup>48</sup> A similar result was observed for pyrene **4**, *i.e.*, sublimation occurred at 2.5 mbar and 50 °C (Fig. S18 and S19†). Such mild sublimation conditions (moderate pressure/low temperature) might enable the cost-efficient preparation of large thin films. A more detailed analysis of the sublimation properties, *i.e.*, determination of the vapor pressure, and preparation of thin films with a single domain of **1** and **4** will be the subject of future work.

## Conclusions

We have reported that structurally simple pyrene molecules **1** and **4**, which bearing only one small isocyano group, exhibit luminescent mechanochromism. Upon exposure to mechanical stress, **1** showed a blue-shifted emission band as a result of a crystal-to-crystal phase transition, while **4** exhibited a red-shifted emission as a result of amorphization. The crystal-structure analyses of **1** and **4** indicated that the change in the strength of the dipole–dipole interactions with neighboring molecules is the origin of their opposite emission-color changes. The low molecular weight of these compounds enables their sublimation under mild conditions (2.5 mbar and 40–50 °C). This study thus offers a new molecular-design strategy to obtain mechanochromic compounds based on the connection of one aromatic core and one small substituent.

## Author contributions

TS designed the project; KH performed and analyzed the experiments with guidance from TS; TS wrote the manuscript.

## Conflicts of interest

There are no conflicts to declare.

## Acknowledgements

This work was financially supported by JSPS KAKENHI grants JP22H021550 and JP22K190580 as well as JST, PRESTO grant JPMJPR21AB (Japan).

## Notes and references

- Z. Chi, X. Zhang, B. Xu, X. Zhou, C. Ma, Y. Zhang, S. Liu and J. Xu, *Chem. Soc. Rev.*, 2012, **41**, 3878–3896.
- Y. Sagara and T. Kato, *Nat. Chem.*, 2009, **1**, 605–610.
- Y. Sagara, S. Yamane, M. Mitani, C. Weder and T. Kato, *Adv. Mater.*, 2016, **28**, 1073–1095.
- S. Xue, X. Qiu, Q. Sun and W. Yang, *J. Mater. Chem. C*, 2016, **4**, 1568–1578.
- S. Mataka, H. Moriyama, T. Sawada, K. Takahashi, H. Sakashita and M. Tashiro, *Chem. Lett.*, 1996, **25**, 363–364.
- S. Mizukami, H. Houjou, K. Sugaya, E. Koyama, H. Tokuhisa, T. Sasaki and M. Kanetsato, *Chem. Mater.*, 2005, **17**, 50–56.
- Y. Sagara, T. Mutai, I. Yoshikawa and K. Araki, *J. Am. Chem. Soc.*, 2007, **129**, 1520–1521.
- H. Ito, T. Saito, N. Oshima, N. Kitamura, S. Ishizaka, Y. Hinatsu, M. Wakeshima, M. Kato, K. Tsuge and M. Sawamura, *J. Am. Chem. Soc.*, 2008, **130**, 10044–10045.
- T. Seki, Y. Takamatsu and H. Ito, *J. Am. Chem. Soc.*, 2016, **138**, 6252–6260.
- M. Jin, T. Seki and H. Ito, *Chem. Commun.*, 2016, **52**, 8083–8086.
- B. Huitorel, H. E. Moll, M. Cordier, A. Fargues, A. Garcia, F. Massuyeau, C. Martineau-Corcus, T. Gacoin and S. Perruchas, *Inorg. Chem.*, 2017, **56**, 12379–12388.
- B. Huitorel, R. Utrera-Melero, F. Massuyeau, J. Mevelec, B. Baptiste, A. Polian, T. Gacoin, C. Martineau-Corcus and S. Perruchas, *Dalton Trans.*, 2019, **48**, 7899–7909.
- Z. Wang, F. Yu, W. Chen, J. Wang, J. Liu, C. Yao, J. Zhao, H. Dong, W. Hu and Q. Zhang, *Angew. Chem., Int. Ed.*, 2020, **59**, 17580–17586.
- S. J. Yoon and S. Y. Park, *J. Mater. Chem.*, 2011, **21**, 8338–8346.
- T. Seki, K. Kobayashi, T. Mashimo and H. Ito, *Chem. Commun.*, 2018, **54**, 11136–11139.
- R. Yoshida, T. Tachikawa and S. Ito, *Cryst. Growth Des.*, 2021, **22**, 547–558.
- T. Ishi-i, H. Tanaka, R. Kichise, C. Davin, T. Matsuda, N. Aizawa, I. S. Park, T. Yasuda and T. Matsumoto, *Chem.–Asian J.*, 2021, **16**, 2136–2145.
- S. Yagai, S. Okamura, Y. Nakano, M. Yamauchi, K. Kishikawa, T. Karatsu, A. Kitamura, A. Ueno, D. Kuzuhara, H. Yamada, T. Seki and H. Ito, *Nat. Commun.*, 2014, **5**, 4013.
- T. Seki, N. Tokodai, S. Omagari, T. Nakanishi, Y. Hasegawa, T. Iwasa, T. Taketsugu and H. Ito, *J. Am. Chem. Soc.*, 2017, **139**, 6514–6517.
- Y. Sagara, S. Yamane, T. Mutai, K. Araki and T. Kato, *Adv. Funct. Mater.*, 2009, **19**, 1869–1875.
- P. Xue, B. Yao, X. Liu, J. Sun, P. Gong, Z. Zhang, C. Qian, Y. Zhang and R. Lu, *J. Mater. Chem. C*, 2015, **3**, 1018–1025.
- H. Tanikubo, T. Matsuo and S. Hayashi, *Bull. Chem. Soc. Jpn.*, 2023, **96**, 178–182.
- T. Wang, N. Zhang, K. Zhang, J. Dai, W. Bai and R. Bai, *Chem. Commun.*, 2016, **52**, 9679–9682.
- E. Nagata, T. Ara and H. Nakano, *Dyes Pigm.*, 2017, **141**, 48–52.
- Q. Kong, W. Zhuang, G. Li, Y. Xu, Q. Jiang and Y. Wang, *New J. Chem.*, 2017, **41**, 13784–13791.
- X. Su, Y. Ji, W. Pan, S. Chen, Y.-M. Zhang, T. Lin, L. Liu, M. Li, Y. Liu and S. X.-A. Zhang, *J. Mater. Chem. C*, 2018, **6**, 6940–6948.
- F. Donati, A. Pucci, C. Cappelli, B. Mennucci and G. Ruggeri, *J. Phys. Chem. B*, 2008, **112**, 3668–3679.



- 28 N. Mizoshita, T. Tani and S. Inagaki, *Adv. Mater.*, 2012, **24**, 3350–3355.
- 29 M. P. Aldred, G.-F. Zhang, C. Li, G. Chen, T. Chen and M.-Q. Zhu, *J. Mater. Chem. C*, 2013, **1**, 6709–6718.
- 30 Unsubstituted anthracene shows luminescent mechanochromism only at low temperature; for details, see: F. Kannen, M. Nishimura, K. Yoza and T. Kusakawa, *Tetrahedron*, 2023, **149**, 133710.
- 31 Pyrene molecules with one bis(pinacolato)diboryl or alkoxy carbonyl group represent another simple molecular design for luminescent mechanochromism; for details, see: ref. 23 and 25.
- 32 K. Kato, T. Seki and H. Ito, *Inorg. Chem.*, 2021, **60**, 10849–10856.
- 33 X. Y. Wang, J. Zhang, J. Yin and S. H. Liu, *Chem.–Asian J.*, 2019, **14**, 2903–2910.
- 34 Y. Sagara, T. Muramatsu and N. Tamaoki, *Crystals*, 2019, **9**, 92.
- 35 Similar to the emission spectra, the solid-state UV-vis absorption spectra of **1** has the onset and peak at a longer wavelength compared to those of **4** (Fig. S4). This could be due to the stronger intermolecular interactions of the former relative to the latter even in the ground state.
- 36 S. K. Rajagopal, A. M. Philip, K. Nagarajan and M. Hariharan, *Chem. Commun.*, 2014, **50**, 8644–8647.
- 37 A. M. Philip, S. K. Manikandan, A. Shaji and M. Hariharan, *Chem.–Eur. J.*, 2018, **24**, 18089–18096.
- 38 T. Seki, K. Kashiyaama and H. Ito, *Dalton Trans.*, 2019, **48**, 7105–7109.
- 39 T. Seki and D. Korenaga, *Chem.–Eur. J.*, 2023, **29**, e202302333.
- 40 The coexistence of two different molecular arrangements in **1** is supported by the observed “intermediate” powder sample prepared by heating (Fig. S12c).
- 41 T. Seki, K. Sakurada and H. Ito, *Chem. Commun.*, 2015, **51**, 13933–13936.
- 42 M. Jin, T. Seki and H. Ito, *J. Am. Chem. Soc.*, 2017, **139**, 7452–7455.
- 43 P. Xue, J. Sun, P. Chen, P. Wang, B. Yao, P. Gong, Z. Zhang and R. Lu, *Chem. Commun.*, 2015, **51**, 10381–10384.
- 44 Z. Lin, X. Mei, E. Yang, X. Li, H. Yao, G. Wen, C.-T. Chien, T. J. Chow and Q. Ling, *CrystEngComm*, 2014, **16**, 11018–11026.
- 45 F. Würthner, *Acc. Chem. Res.*, 2016, **49**, 868–876.
- 46 Unfortunately, the single-crystal X-ray diffraction analysis of a thermally obtained crystal of **1**<sub>after</sub> was inconclusive, most likely due to the proximity of the thermal phase-transition temperature of **1** (100 °C) to its melting point (130 °C; Fig. S13).
- 47 For structurally simple luminescent pyrene molecules without mechanochromic properties, see: ref. 36. For mechanochromic compounds with low molecular weight (MW = 218–271), see: refs. 16, 43, and 44.
- 48 Under these conditions, the single crystallinity of the sublimated samples of **1** could not be confirmed.

